PARAMETRIC STUDY OF THE HEAT TRANSFER COEFFICIENT IN BI-DIMENSIONAL SMOLDERING SIMULATION

by

Chekib GHABI, Hmaied BENTICHA, and Mohammed SASSI

Original scientific paper
UDC: 662.636/.638:66.011
BIBLID: 0354-9836, *11* (2007), 4, 95-112

In this paper, we present the transient modeling results of 2-D forward smoldering in a cylindrical configuration filled with a foam porous material. The objective of the study is to explain the effect of the heat losses from lateral boundaries in the front smolder propagation. The developed numerical code is capable of predicting the fire initiation and the smoldering (slow-burning) characteristics of foam insulation materials. The finite volume discretization and the bi-conjugate gradient stabilized method are used to solve the system governing equations. The chemical kinetics model is based on a first order pyrolysis reaction, followed by oxidation of the porous fuel and the carbonaceous char residual. This second oxidation reaction might promote the transition from smoldering to flaming and thus fire initiation. The gas and solid temperature, and the oxygen and the char mass fraction two-dimensional temporal evolutions are computed. Different heat and mass transfer coefficients are used to simulate the heat losses to the surrounding. Non-reacted foam regions are observed near the side wall, confirming experimental observations. The base case is chosen to represent the experimental conditions reported in the literature. The numerical predictions show very good agreement with the published experimental and 1-D numerical results.

Key words: *smoldering, fixed bed, heat transfer, porous medium, finite volume method, bi-conjugate gradient stabilized method*

Introduction

Smoldering is a flameless burning process that can occur in charring fuels, such as wood, cigarettes, and expanded polymers. The combustion reaction is heterogeneous and occurs in the interior or on the surface of the porous fuel. There has been a growing interest in the smoldering, because of environmental and fire safety concerns. Smoldering can generate significant air pollutants, cause biomass consumption, and may also initiate new fires. Smoldering combustion proceeds by a process of pyrolysis, producing volatile products and a solid char; then the solid char in turn oxidizes with diffusing oxygen to produce the heat that keeps the whole process self-sustaining.

Smoldering is defined as a non-flaming, self sustaining, propagating, exothermic, surface reaction; deriving its principal heat from heterogeneous oxidation of a po-

rous solid fuel [1, 2]. From a practical point of view, smoldering presents a serious fire risk because the reaction can propagate slowly in the material interior and can go undetected for long periods of time. Therefore, it is at least necessary to prevent the smoldering from transiting to flaming combustion. Ohlemiller [1, 2] provided two extensive reviews of experimental and theoretical studies of smoldering; and they argue that since the oxidizer flows through the porous char, it has to be totally consumed for the smoldering reaction to propagate. Ohlemiller [1] interpreted forward smolder as a thermal wave followed by a char oxidation reaction.

Torero and Fernandez-Pello [3] conducted an experimental study of forward smolder of polyurethane foam in air, along with a 1-D simulation of the phenomenon. They observed that the char was not totally consumed by the flowing oxidizer. Later, Torero *et al.* [4] gave a phenomenological interpretation of their observation based on different char reactivities. Tse *et al.* [5] presented results in agreement with these phenomenological explanations. Dosanjh *et al*. [6] developed a theoretical model of forward smolder through a porous solid fuel, and they have examined the conditions for a steady smolder front and for the transition to extinction. In their analysis they consider air and fuel moving into the reaction zone. Their model is based on two reactions: a non-oxidative pyrolysis reaction where the fuel is decomposed into char and volatile matter, followed by a second reaction of char oxidation.

Buckmaster and Lozinski [7] developed a similar model providing a more elaborate description of the structure of the oxidation and pyrolysis fronts. Leach *et al*. [8] extended the 1-D model to transient cases to model the experimental configuration and explain the observations of Torero and Fernandez-Pello [3]. They considered separate gas and solid phase energy equations with two other equations for oxygen conservation, one in the bulk and the other at the solid surface. Their resulting equations were solved numerically by the finite-difference technique using the VODE numerical code. Effects of several parameters including kinetic parameters, thermophysical properties, oxygen concentration and fuel bed porosity were studied. Relatively good agreement was obtained between the experimental and the numerical results. In an earlier work, Leach *et al*. [8] used the same numerical technique for modeling reverse smoldering of a porous fuel bed.

In our work on reverse combustion of a fixed porous bed, we have developed a 2-D numerical code for fuel consumption rate predictions as a tool for burner design [9]. Also Ghabi *et al.* [10, 11] have extend this numerical simulation to predict the 2-D smoldering of polyurethane based on the Leach model of chemical kinetic. At the same time Bar-Ilan *et al.* [12] presented experimental results from two forward forced-flow smolder tests on polyurethane foam using air as oxidizer conducted aboard the NASA space shuttle. Their experimental results revealed regions of non-reacted foam near the side wall which their 1-D model could not predict and estimate its effect on the smolder propagation velocity.

Di Blasi [13] refined the kinetic model of the smoldering of a wood slab under thermal radiation on one face. Effects of variable thermophysical properties, unsteady gas phase processes, pressure and velocity variations and convective transport of tar species were accounted for. The secondary reactions from tar to char and gas were also included in the model.

A comprehensive review of modeling and simulation techniques for the combustion of charring and non-charring solid fuels has been presented by Di Blasi [14]. Reliable kinetic data for thermal degradation and oxidation of biomass materials are limited, especially for oxidation. Most of the modeling works mentioned above have used the kinetic data provided by Kashiwagi and Nambu [15] for a cellulose paper. Shafizadeh and Bradbury [16] presented other sources of kinetic data.

Chao and Wang [17] studied experimentally the transition of the smoldering to the flaming phase of polyurethane foam under natural convection conditions. They showed that this transition is the result of the oxidization of the char. Then Wang *et al.* [18] studied the effect of smoldering under forced convection conditions, where they adopted a kinetics model with two reactions, and they included the radial effect on the smoldering propagation.

Bilbao *et al*. [19] have worked on the smoldering of wood, and they have conducted several experiments in an instrumented combustion chamber. They proved that reactional kinetics is dependent on temperature, and they specified a set of kinetics parameters for each limited temperature interval.

Shult *et al*. [20] employed asymptotic methods to find a smolder wave solution with two different structures, a reaction leading wave structure when the velocity of the combustion layer exceeds that of the heat transfer layer, and a reaction trailing wave structure obtained when the combustion layer is slower than the heat transfer layer. These qualitative theoretical descriptions agreed with Ohlemiller [1] explanations and Torero *et al*. [4] experimental observations.

This work is, therefore, an effort to develop a comprehensive numerical simulation code for a 2-D smoldering prediction. The Bar-Ilan *et al*. [12] base case of forward smoldering in a cylindrical configuration filled with a porous material is investigated using the finite volume modeling (FVM) along with the bi-conjugate gradient stabilized (bi-CGStab) algorithm. The solid and gas temperatures, the oxygen mass fractions in the bulk and on the solid surface, as well as the char mass fraction temporal evolutions are computed. The obtained numerical results are then compared to the numerical results of Leach *et al.* [21], and the experimental observations of Bar-Ilan *et al.* [12].

This work provides information on the 2-D temperature and char mass fraction distributions that previous smolder modeling works did not predict. The way that the transient effects are included in this work makes it distinguishable from works as described elsewhere in this paper. A parametric study is producted to predict the heat losses from the lateral wall. The thermal boundary conditions used in this analysis are more practical than any other modeling work available in the literature.

Model description

Figure 1 shows a scheme of the studied configuration. A fixed bed of foam, with a length of 15 cm and a radius of 15 cm in size is utilized. For simplicity, we assume that the char and ash have the same properties, and the gas formed from the pyrolysis and oxidation reactions leaves the bed before reacting. Initially, the entire domain is consisting

of unreacted foam fuel. Air flows into the left face of the foam material, and the smoldering process is initiated by maintaining a specified high temperature or by applying a high heat flux at this surface for a certain period of time until self-propagation is obtained. We assume also that the reaction zone propagates from the left to the right of the fuel bed, and the gravitational effects are neglected to permit comparison with the microgravity experimental results.

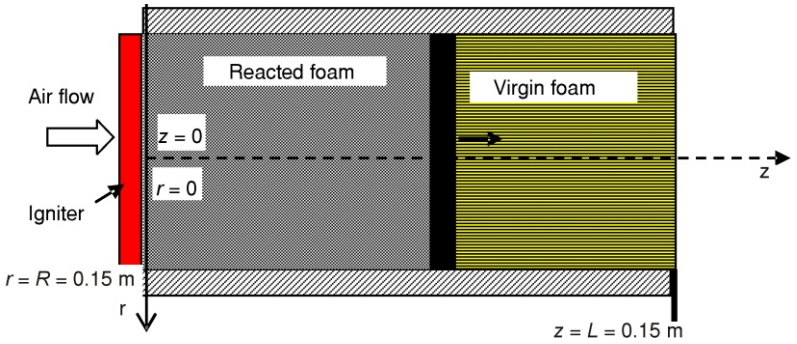

Figure 1. Forward smoldering configuration

Mathematical model

The mathematical model is based on the energy and mass conservation equations.

Reaction kinetics

The kinetics model used in this study and which is summarized in the following is based on three reactions for the char formation and oxidation [1], which is reported by Ghabi *et al*. [10,11] with rates of production and consumption of mass which are similar to those given by Kashiwagi and Nambu [15], and Leach *et al*. [8]

Exothermic oxidation of foam

$$1\,\mathrm{g(fuel)} \quad n_{\mathrm{ol}}\mathrm{O_2} \quad n_{\mathrm{cl}}\,\mathrm{(char)} \quad n_{\mathrm{gl}}\,\mathrm{(gas)} \tag{1}$$

$$w_{\mathrm{ox}} \quad (1 \quad Y_{\mathrm{c}} \quad Y_{\mathrm{a}})^{f}\rho_{\mathrm{s}}A_{\mathrm{ox}}(Y_{\mathrm{O_2}})^{m}\mathrm{e}^{\frac{E_{\mathrm{ox}}}{\mathrm{R}T_{\mathrm{s}}}} \tag{2}$$

Endothermic reaction of pyrolysis

$$1\,\mathrm{g(fuel)} \quad n_{\mathrm{c2}}\,\mathrm{(char)} \quad n_{\mathrm{g2}}\,\mathrm{(gas)} \tag{3}$$

$$w_{\mathrm{py}} \quad (1 \quad Y_{\mathrm{c}} \quad Y_{\mathrm{a}})^{g}\rho_{\mathrm{s}}A_{\mathrm{py}}\mathrm{e}^{\frac{E_{\mathrm{py}}}{\mathrm{R}T_{\mathrm{s}}}} \tag{4}$$

Exothermic oxidation of the char

$$1\,\mathrm{g(char)} \quad n_{o3}\mathrm{O_2} \quad n_{a3}\,(\mathrm{ash}) \quad n_{g3}\,(\mathrm{gas}) \tag{5}$$

$$w_a \quad Y_c \rho_c A_a (Y_{O_2})^h \mathrm{e}^{\frac{E_a}{RT_s}} \tag{6}$$

Conservation equations

Mass conservation equation

$$\frac{\partial(\varepsilon\rho_g)}{\partial t} \quad \frac{1}{r}\frac{\partial(r\varepsilon\rho_g u_r)}{\partial r} \quad \frac{\partial(\varepsilon\rho_g u_z)}{\partial z} \quad \varepsilon[(n_{g2} \quad n_{ol})w_{ox} \quad n_{g2}w_{py} \quad (n_{g3} \quad n_{o3})w_a] \tag{7}$$

Oxygen conservation equation in the volume of gas

$$\frac{\partial(\varepsilon\rho_g Y_{O_2})}{\partial t} \quad \frac{1}{r}\frac{\partial(r\varepsilon\rho_g u_r Y_{O_2})}{\partial r} \quad \frac{\partial(\varepsilon\rho_g u_z Y_{O_2})}{\partial z}$$

$$\frac{1}{r}\frac{\partial}{\partial r} \; r\rho_g D_{\mathrm{eff}\,g}\frac{\partial}{\partial r}(Y_{O_2}) \quad \frac{\partial}{\partial z} \; \rho_g D_{\mathrm{eff}\,g}\frac{\partial}{\partial z}(Y_{O_2}) \quad k_m S(Y_{O_2 s} \quad Y_{O_2}) \tag{8}$$

Oxygen conservation equation at the reaction surface

$$\frac{\partial(\varepsilon_s\rho_g Y_{O_2 s})}{\partial t} \quad \frac{1}{r}\frac{\partial}{\partial r} \; r\rho_g D_{\mathrm{eff}\,s}\frac{\partial}{\partial r}(Y_{O_2 s}) \quad \frac{\partial}{\partial z} \; \rho_g D_{\mathrm{eff}\,s}\frac{\partial}{\partial z}(Y_{O_2 s})$$

$$k_m S(Y_{O_2} \quad Y_{O_2 s}) \quad n_{ol}w_{ox} \quad n_{o3}w_a \tag{9}$$

Energy conservation equation in the gas phase

$$\frac{\partial(\varepsilon\rho_g Cp_g T_g)}{\partial t} \quad \frac{1}{r}\frac{\partial(r\varepsilon\rho_g u_r Cp_g T_g)}{\partial r} \quad \frac{\partial(\varepsilon\rho_g u_z Cp_g T_g)}{\partial z}$$

$$\frac{1}{r}\frac{\partial}{\partial r} \; r\lambda_{g\,\mathrm{eff}}\frac{\partial}{\partial r}(T_g) \quad \frac{\partial}{\partial z} \; \lambda_{g\,\mathrm{eff}}\frac{\partial}{\partial z}(T_g) \quad h_{gs}(T_s \quad T_g) \tag{10}$$

Species conservation equations in the solid phase

$$\frac{\partial(\rho_s Y_c)}{\partial t} \quad n_{cl}w_{ox} \quad n_{c2}w_{py}w_a \tag{11}$$

$$\frac{\partial(\rho_c Y_a)}{\partial t} \quad n_{a3}w_a \tag{12}$$

Energy conservation equation in the solid phase

$$\frac{\partial(\rho_s Cp_s T_s)}{\partial t} \quad \frac{1}{r}\frac{\partial}{\partial r} \; r\lambda_{s\,\mathrm{eff}}\frac{\partial}{\partial r}(T_s) \quad \frac{\partial}{\partial z} \; \lambda_{s\,\mathrm{eff}}\frac{\partial}{\partial z}(T_s) \quad h_{gs}(T_g \quad T_s) \quad \dot{Q}_{\mathrm{rad}}$$
$$w_{ox}\Delta H_{ox} \quad w_{py}\,\Delta H_{py} \quad w_a \Delta H_a \tag{13}$$

with

$$Q_{\mathrm{rad}} \quad \mathrm{div}\{ \; \lambda_{\mathrm{rad}}[\overline{\mathrm{grad}}(T_s)]\} \tag{14}$$

The ideal gas equation of state is used to account for the gas density. These last two equations account for the oxygen diffusion in the bulk and at the solid surface. Heat transfer between the solid and the gas is obviously similar to mass transport between the solid and the bulk gas. The chemical reaction occurring at the surface of the fuel depends on the concentration and on the adsorption of oxygen. We assume that the dissociation of the oxygen molecule on the surface depends only on the activation energy and the internal solid porosity. In eq. (3), we assume that the gas velocity at the surface is equal to zero, consequently the second term of the first member of this equation vanishes.

The axial pressure gradient in the porous media is calculated by the Ergun's law [22] as a function of the void fraction:

$$\frac{\partial P}{\partial z} \quad \frac{150\mu_g(1 \quad \varepsilon)^2}{d_p^2\varepsilon^3}u_z \quad \frac{\rho_g(1 \quad \varepsilon)}{d_p\varepsilon^3}u_z^2 \tag{15}$$

The radial pressure gradient variation is neglected.

Transport coefficients and properties

The volumetric heat transfer coefficient between the gas and the solid is calculated as a function of Reynolds and Prandtl numbers, based on a Nusselt number correlation from [23]:

$$\mathrm{Nu} \quad \frac{h_{gs}d_p}{\lambda_{g\,\mathrm{eff}}} \quad 2 \quad 1.1\sqrt[3]{\mathrm{Re}^2\,\mathrm{Pr}} \tag{16}$$

where d_p is the pore diameter, and $\lambda_{g\,\mathrm{eff}}$ is the gas thermal effective conductivity.

The specific surface of exchange between the solid and the gas is defined as:

$$S \quad \frac{4(1 \quad \varepsilon)}{d_p} \tag{17}$$

The volumetric mass transfer coefficient is, however, determined by analogy to heat transfer according to Incropera and DeWitt [24]:

$$\frac{h_{gs}}{k_m} \quad \rho_g Cp_g \mathrm{Le}^{(1 \quad n)} \tag{18}$$

where Le (= α/D) is the Lewis number, and for most applications they signaled that is reasonable to use (n = 1/3).

The effective diffusivity coefficients were calculated by Ghabi *et al*. [11] approximations:

$$D_{\mathrm{g\,eff}} \quad \varepsilon D_0 \sqrt{\frac{T_{\mathrm{g}}}{T_{\mathrm{g0}}}}^{3} \tag{19}$$

$$D_{\mathrm{s\,eff}} \quad (1 \quad \varepsilon) D_0 \sqrt{\frac{T_{\mathrm{s}}}{T_{\mathrm{s0}}}}^{3} \tag{20}$$

The mass fraction of the solid and the variation of its physical properties are calculated from the mass fraction of char and ash. The char oxidation into ash takes place at a high temperature that can initiate flaming of the material. When this happens, the settings of this smoldering study are modified. For simplicity, the physical properties of the char and the ash are assumed as being identical. The effect of the radiation heat transfer is modeled by the Rosseland approximation presented in [24], by introducing a radiation conductivity, such that the total thermal conductivity of the solid is given by:

$$\lambda_{\mathrm{s}} \quad (Y_{\mathrm{c}} \quad Y_{\mathrm{a}})\lambda_{\mathrm{c}} \quad (1 \quad Y_{\mathrm{c}} \quad Y_{\mathrm{a}})\lambda_{s0} \tag{21}$$

$$\lambda_{\mathrm{rad}} \quad \frac{16\sigma d_{\mathrm{p}} T_{\mathrm{s}}^{3}}{3} \tag{22}$$

$$\lambda_{\mathrm{s\,eff}} \quad (1 \quad \varepsilon)\lambda_{\mathrm{s}} \quad \lambda_{\mathrm{rad}} \tag{23}$$

The used thermophysical and chemical parameters along with other input parameters of the simulation are summarized in tab. 1.

Initial and boundary conditions

Initially, the left face of the cylindrical foam material, which is represented on fig. 1, is heated by an igniter. The temperature of this face is increased exponentially from 300 to 680 K for 500 s. When the smolder wave is initiated and the peak temperature of the foam occurs, and when the smolder wave moves away from the igniter for over 2-3 cm, the igniter is turned off and the smolder self propagates from the left to the right.

Initial conditions

– At t = 0 s

$Y_c = Y_a = 0$, $Y_s = 1$, $T_g = T_s = 300$ K (24)

Boundary conditions

– At the axis of the sample

Table 1. Input parameters of the numerical simulation

Property	Value	Reference	Property	Value	Reference
λ_{s0}	$6.3\cdot10^{-2}$ W/mK	[14]	T_{amb}	300 K	
d_p	$5\cdot10^{-5}$ m	[25]	P_{amb}	$1.013\cdot10^{5}$ Pa	
ρ_c	10 kg/m^3	[4, 12]	ΔH_{ox}	–5700 J/g	[15]
ρ_s	26.5 kg/m^3	[4, 12]	ΔH_{py}	500 J/g	[15]
Cp_s	1.7 kJ/kgK	[4, 12]	ΔH_a	–25.000 J/g	[15]
Cp_c	1.1 kJ/kgK	[4, 12]	n_{o1}	0.41	[15]
λ_g	$2.58\cdot10^{-2}$ W/mK	[13]	n_{c1}	0.21	[15]
ε	0.975	[4, 12]	n_{c2}	0.24	[15]
ε_s	$5\cdot10^{-3}$	[11]	n_{o3}	1.65	[15]
D_0	$4.53\cdot10^{-5}$ m^2/s	[4, 12]	n_{a3}	0.03	[15]
u_{in}	$5.3\cdot10^{-3}$ m/s	[4, 12]	E_{ox}/R	19.245 K	[15]
h_s	0.70 W/m^{2}K	[11]	E_{py}/R	26.500 K	[15]
h_{ws}	0.07-0.1 W/m^{2}K	varied	E_a/R	19.244 K	[15]
h_{wg}	0.07-0.1 W/m^{2}K	varied			

The cylindrical revolution symmetry is assumed:

$$\left.\frac{\partial \Phi}{\partial r}\right|_{r\ 0} \quad 0 \tag{25}$$

where

$$\Phi \quad \{Y_c, Y_a, Y_s, Y_{O_2}, Y_{O_2 s}, T_g, T_s\}$$

– At the sidewall of the sample

The sidewall is considered to be impermeable of matter:

$$\left.\frac{\partial \Phi}{\partial r}\right|_{r\ R} \quad 0 \tag{26}$$

where

$$\Phi \quad \{Y_c, Y_a, Y_s, Y_{O_2}, Y_{O_2 s}, T_g, T_s\}$$

For the temperature the boundary conditions are described by the second type of conditions:

$$\lambda_{s\,\mathrm{eff}} \left.\frac{\partial T_s}{\partial r}\right|_{r\ R} \quad h_{w\,s}(T_\infty \quad T_s) \tag{27}$$

$$\lambda_{g\,\mathrm{eff}} \left.\frac{\partial T_g}{\partial r}\right|_{r\ R} \quad h_{w\,s}(T_\infty \quad T_g) \tag{28}$$

– At left face
Before the igniter is shut down:

$$T_g = 300\ \text{K}, \qquad T_s = T_{\text{igniter}} \tag{29}$$

After the igniter is shut down:

$$T_g \quad 300\ \text{K}, \quad \lambda_{s\,\text{eff}} \frac{\partial T_s}{\partial r} \qquad h_s(T_s \quad T_\infty) \tag{30}$$

– At the right face
In this face, the established regime is considered:

$$\frac{\partial \Phi}{\partial z}_{z\ H} \qquad 0 \tag{31}$$

where

$$\Phi \quad \{Y_{O_2}, Y_{O_2 s}, T_g, T_s\}$$

Numerical method

For the numerical simulation, the finite volume method in cylindrical coordinates with an upwind scheme is used to discretize the governing equations. This method has been extensively used in several engineering applications. It is quite attractive when modeling problems for which the flux is of importance, such as in fluid mechanics, or in heat and mass transfer.

The numerical method applied to solve the model was the finite volume method exclusively described by Patankar [26]. After the integration, the discretized equations for each control volume were written in a matrix forming a system of algebraic equations:

$$A_p\Phi_p = A_w\Phi_w + A_e\Phi_e + A_n\Phi_n + A_s\Phi_s + S_\Phi \tag{32}$$

The obtained system of discretized equations is resolved by the method of Bi-CGStab preconditioned (left and right preconditioning) as described by Markovic [27]. In addition to stability and computation time, accuracy of the solution also plays an important role in choosing the right mesh size. We give particular attention to accuracy analyses of the results. In this work we have used the grid (150×150). In order to reduce the CPU time needed for the resolution, a variable time step is used as: $\Delta t = 10^{-2}$ s for $t < 500$ s, and $\Delta t = 10^{-4}$ s for all $t > 500$ s. As a result and when using a Pentium 4, with 512 MB of RAM and 64 MB of cash memory, the CPU time for our 2-D computations was about 47 hours. However, Hanneke and Ellzey [28] for resolving the same system of equations in their 1-D model with the DVODE integrator proposed by Leach *et al*. [21], indicated a CPU time on an IBM RS/6000 of 90 hours.

The BiCGStab method proved to be very efficient with the sparse matrix nature of the obtained equations. Sparse matrix computations need special attention. Such com-

putations occur frequently in scientific calculations. The typical development path for sparse matrix applications involves picking a needed algorithm, selecting a sparse data structure, and then implementing the specific algorithm using the selected sparse data structure.

In order to optimize the use of RAM, the Yale Sparse Matrix Package "YSMP" technique was used for matrix storage. This technique is described in [29, 30].

Results and discussion

We recall that the main objective of this 2-D numerical simulation study is to predict the two-dimensional nature of the post-flight images of the foam samples from the forced forward microgravity smoldering tests reported by Bar-Ilan *et al*. [12], and which showed non-reacted foam near the side wall. The results are also compared to Leach *et al.* [21] numerical results for axial evolutions and validated in [11].

Temperature evolution in the medium

In this section, the solid and gas temperature distributions in the medium are analyzed. The heat coefficient $h_{ws} = 0.07$ W/m^{2}K is supposed. For the solid phase. The solid temperature field is analyzed at different steps of the smolder propagation, which are represented at the times: $t = 1100$, 1250, 1500 , and 1530 s. Figures 2a-d show the isothermal values of the solid phase temperature at the four instants, respectively. These figures show a curvature in the smolder zone near the side wall, and a hot zone near the axis which is larger than the one near the wall. This is due to the heat losses from the reaction zone to the wall. Consequently a non reacting zone is observed near the wall, which is indicated by a low temperature region.

The heat released by the heterogeneous oxidation (smolder) reaction is transferred axially ahead and radially of the reaction zone by conduction, convection and radiation, heating the unreacted foam fuel. The resulting increase in the fresh fuel temperature leads successively to pyrolysis, solid fuel oxidation and then to the onset of the char oxidation, and consequently gives way to the smolder wave propagation through the foam. Near the side wall, part of this heat is lost and the propagating reaction would leave behind a char that contains a significant amount of unreacted fuel as will be shown later on the char mass fraction field evolutions.

These last figures also show that as the smolder wave propagates, the peak temperatures remain within ranges typical of smoldering, and the maximum temperature increases slowly in both the axial and radial directions. This can cause flaming combustion for a long bed, when the heat release from the exothermic oxidation is more than the heat consumed by the endothermic pyrolysis. This is clear in fig. 2d when the temperature rises to 750 K near the exit.

For further explanation of this increase of the maximum temperature, the axial solid temperature evolution at the centerline of the foam medium is represented for dif-

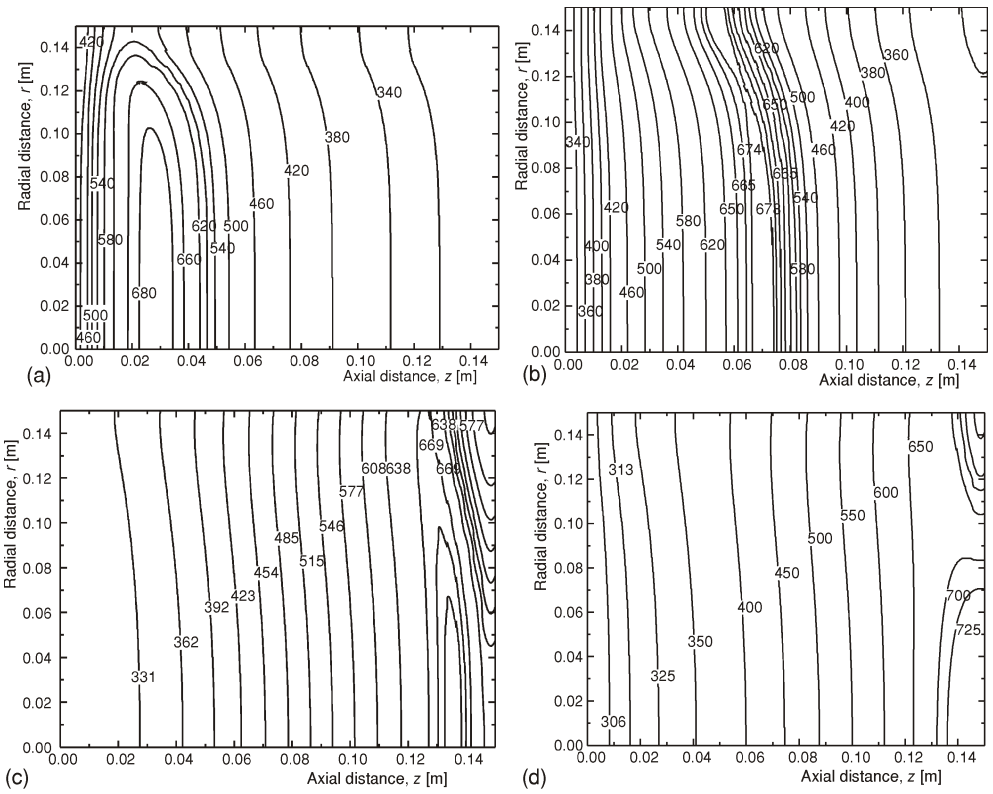

Figure 2. Solid temperature field; *(a) t = 1100 s; (b) t = 1250 s; (c) t = 1500 s; (d) t = 1530 s*

ferent instants of time in fig. 3. This figure shows clearly the propagation of the smolder wave and the increase of the peak temperature.

For the gas phase, the axial gas temperature evolution at the centerline of the foam medium is reported in fig. 4 for different instants. This figure shows that the gas temperature is slightly smaller than the solid temperature. For example the predicted solid-gas temperature difference is of 25 K at 1100 s on the peak. A larger hot zone in the gas phase near the peak is observed than the solid one. This is because the heat is generated in the solid phase as a result of chemical reactions and has to be transferred from the solid to the gas phase through the gas-solid interface. However, the gas temperature shows similar trend as the solid temperature and, as observed for the solid phase, similar increase in the peak temperature for the gas is also observed when the smolder wave propagates from the left to the right.

The simulations revealed that several parameters can influence the ignition and propagation of the smolder wave, such as the frequency factor in the kinetics model, the igniter temperature, the inlet gas velocity, the instant of igniter extinc-

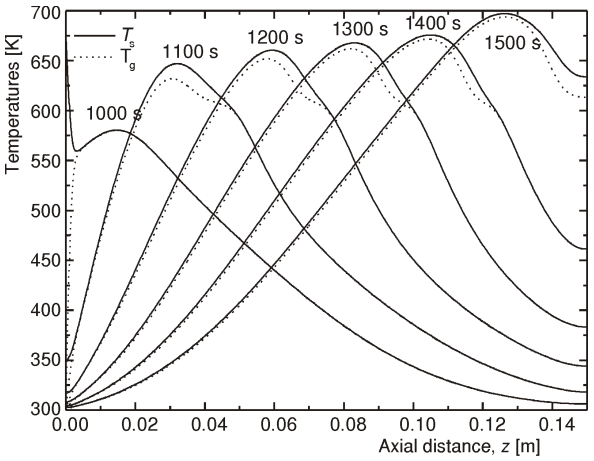

Figure 3. Axial solid and gas temperatures evolution for $r = 0$ cm

tion, and the heat transfer coefficient between the solid and the gas. All of these parameters were optimized for smolder propagation without transition to flaming or extinction before our parametric study on heat losses to the wall was carried. In particular, the kinetic parameters were chosen to insure the stable and repeatable smolder wave propagation for an inlet air velocity of (5.3 mm/s) with an oxygen concentration of (Y_{O_2} 0.23), to permit the comparison with the literature results.

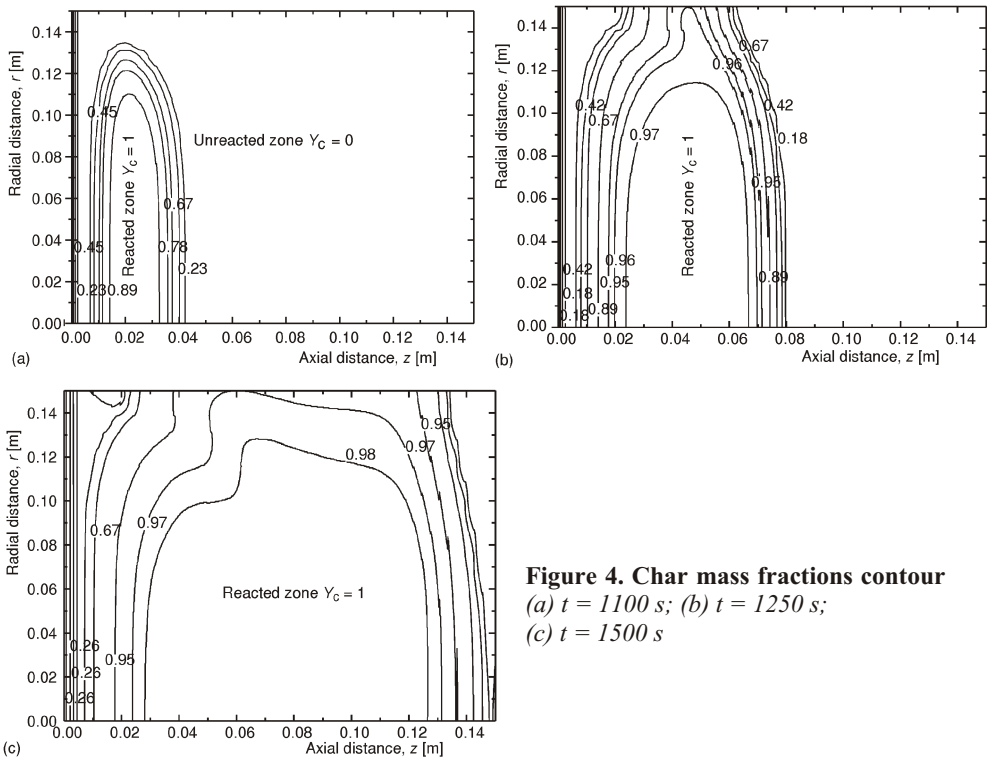

Figure 4. Char mass fractions contour
(a) t = 1100 s; (b) t = 1250 s;
(c) t = 1500 s

Char mass fractions

In this section, the smoldering phenomenon is analyzed through the analysis of the resulting char, which is the product leaved behind after the propagation of the smolder wave front.

Two dimensional char mass fraction distributions are shown on figs. 4a-c where the char conversion contours are presented for t = 1100, 1250, and 1500 s, respectively. It emanates from these figures that the zone of char reaction can be limited between $Y_c = 1$ and $Y_c = 0.1$. These figures show clearly the unreacted zone $Y_c < 0.1$ near the side wall and especially at the inlet and outlet corners where the heat losses are higher to the ambient air, as pronounced on fig. 4c. The presence of this unreacted fuel is justified by the insufficient heat in this zone to convert original foam into char. These char mass fraction distributions are in very good agreement with the post-flight images (fig. 5) reported by Bar-Ilan *et al*. [12].

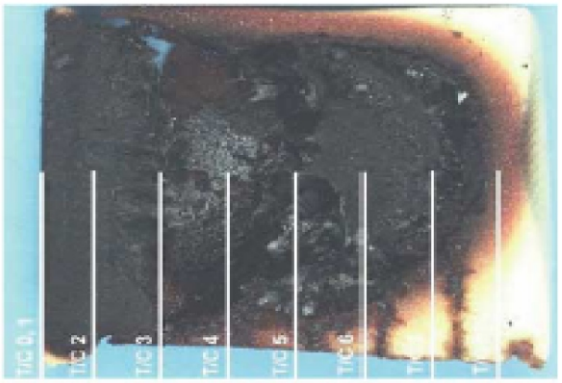

Figure 5. Photographic of char formation in a foam smoldering taken from [12]

Figure 6 shows the axial char mass fraction evolution at the centerline of the cylindrical medium. This evolution is presented for selected time values. Initially, and because of the incoming cold air, very small quantity of char is formed (20% of the initial foam) near the ignition end and a small non converted foam zone appears near the air inlet and especially close to the side wall. Then, as the smolder wave propagates toward the right end, more and more foam is converted into char and the char mass fraction reaches the unity value.

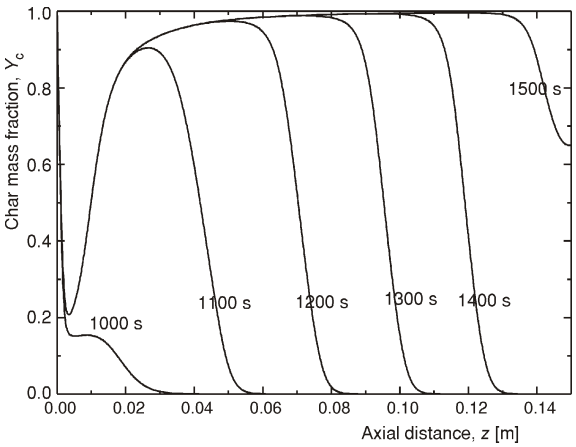

Figure 6. Char mass fractions evolution at the centerline (r = 0 cm)

Effect of the heat transfer coefficient

The effect of the convective heat transfer coefficient between

the solid bed and the environment at $r = R$ is analyzed through four values of h_{ws} (0.07, 0.09, 0.095, and 0.1 W/m^{2}K), and we suppose that $h_{ws} = h_{wg}$. For each of these values, the char mass fraction evolution versus time is presented at a specified axial section for two radial distances, namely at the centerline and at the sidewall.

For $z = 4$ cm, fig. 7 shows that in the centerline, the evolutions of the char mass fractions versus time for different values of h_{ws} are supposed, and then the heat transfer coefficient hasn't any effect. However, at the side wall, the increase of the heat transfer coefficient values decreases the conversion rate and then the char mass fraction. We can also note that the increase of h_{ws} from 0.07 to 0.09 W/m^{2}K, decreases the char mass fraction by about 75%, and that very small char quantity is obtained when increasing h_{ws} to 0.1 W/m^{2}K. Furthermore, the char mass fraction increase more rapidly for the small values of h_{ws} than for the greater ones. Physically, this can be explained by the fact that when using greater values of h_{ws} = 0.1, more heat is released to the environment and then small quantity of foam is converted into char.

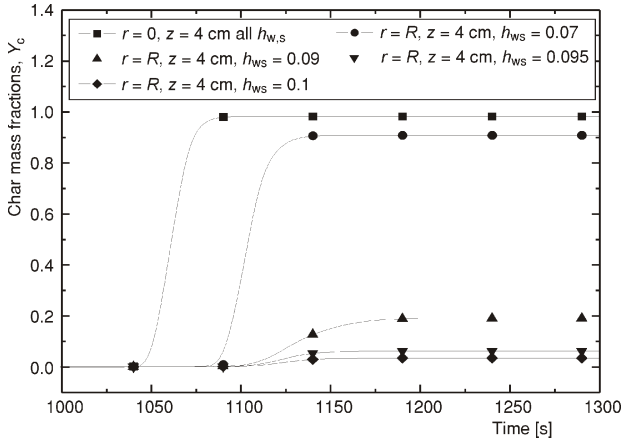

Figure 7. Char mass fractions as a function of time for $z = 4$ cm in the wall bed for different values of heat transfer coefficient

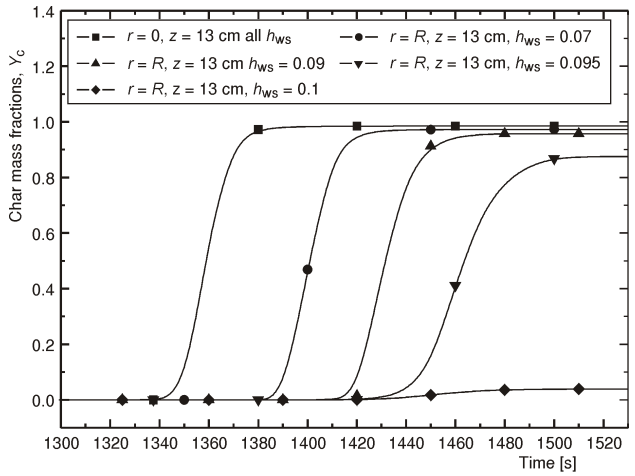

Figure 8. Char mass fractions as a function of time for $z = 13$ cm in the wall bed for different values of heat transfer coefficient

For a section toward the exit, z = 13 cm, similar results are reported in fig. 8. From this figure, the temporal char mass fraction evolution, at the centerline, are again the same. At the side wall, the same effect of the heat transfer coefficient is noted. That is, decreasing char mass fraction occurs

when the heat transfer coefficient h_{ws} increases, but the dramatic decrease occurs when h_{ws} is increased from 0.095 to 0.1 W/m^{2}K. Again, the more rapid conversion of foam into char is noted for small values of h_{ws}.

Smolder velocity

When the smolder wave begins propagating, the smolder wave velocity for the foam is computed at the smolder front. This velocity can be deduced from fig. 3. In fact, having the times when the peak temperatures occur, we can calculate the distance between these peaks, and thus the smolder velocity can be computed for a heat wall coefficient h_{ws} = 0.07 W/m^{2}K.

Therefore, the smolder velocity is arbitrarily defined as the axial traveling velocity of the peak temperature of the smoldering zone and presented in fig. 9. This figure shows that the smoldering phenomenon is initially accelerated, and the velocity decreases slightly toward the right end. The observed average smolder velocity is about 0.25 mm/s in very good agreement with the 0.23 mm/s value observed by Bar-Ilan *et al*. [12]. However, Leach *et al*. [21] for the 1-D simulation and for the same gas velocity reported a smolder velocity of 0.45 mm/s. This could be explained by the 2-D effect where a quantity of the heat release is transferred radially to the sidewall.

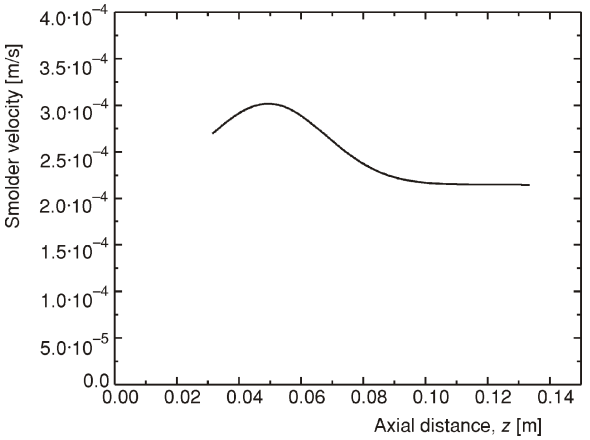

Figure 9. Smolder velocity

Conclusions

A new method for numerical simulation of two-dimensional smoldering propagation in a porous foam bed has been proposed and investigated. This is based on the finite volume discretization and the bi-CGStab technique. The obtained numerical results showed a clear agreement with the experimental numerical results available in the literature. This work provides information on the 2-D temperature and char mass fraction distributions that previous smolder modeling works did not predict. The thermal boundary conditions used in this analysis are more practical than any other smolder simulation studies. The developed code is very versatile and open to simulate any smoldering and/or reacting front propagation through a fixed bed, and especially as related to fire initiation prediction in electrical and/or thermal isolation systems.

Nomenclature

A – frequency factor, [s^{-1}]
Cp – specific heat, [$Jkg^{-1}K^{-1}$]
D – diffusion coefficient, [m^2s^{-1}]
d – diameter, [m]
E – activation energy, [$Jmol^{-1}$]
ΔH – enthalpy of reaction, [Jkg^{-1}]
h – heat transfer coefficient, [$Wm^{-2}K^{-1}$]
k_m – mass transfer coefficient, [ms^{-1}]
n – stoichiometric coefficient, [–]
P – pressure, [Pa]
R – perfect gas constant, [$JK^{-1}mol^{-1}$]
r – radial coordinate, [m]
S – specific surface area, [m^{-1}]
T – temperature, [K]
t – time, [s]
u – gas velocity, [ms^{-1}]
Y – mass fraction, [$kgkg^{-1}$]
w – mass reaction rate, [$kgm^{-3}s^{-1}$]
z – axial coordinate, [m]

Greek symbols

α – thermal diffusivity, [m^2s^{-1}]
ε – porosity, [–]
λ – conductivity, [$Wm^{-1}K^{-1}$]
μ – dynamic viscosity, [$kgm^{-1}s^{-1}$]
σ – Stefan-Bolzman constant (=$5.67\cdot10^{-8}$), [$Wm^{-2}K^{-4}$]
ρ – mass density, [kgm^{-3}]

Subscripts

a – ash, char oxydation
amb – ambiant
c – char
eff – effective value
g – gas
ox – fuel oxidation
p – pore
py – fuel pyrolysis
r – radial direction
rad – radiation
s – solid or surface
z – axial direction

References

[1] Ohlemiller, T. J., Modeling of Smoldering Combustion Propagation, *Progress in Energy and Combustion Science, 11* (1986), 4, pp. 277-310

[2] Ohlemiller, T. J., Smoldering Combustion, in: SFPE Handbook of Fire Protection Engineering, Section 2, Chapter 11, 2nd ed. (Eds., P. J. DiNenno, C. L. Beyler, R. L. P. Custer, W. D. Walton), National Fire Protection Association, Quincy, Mass, USA, 1995, 2/171-179
[3] Torero, J. D., Fernandez-Pello, A. C., Forward Smolder of Polyurethane Foam in a Forced Air Flow, *Combustion and Flame, 106* (1996), 1-2, pp. 89-109
[4] Torero, J. L., Fernandez-Pello, A. C., Kitano, M., Opposed Forced Flow Smoldering of Polyurethane Foam, *Combustion Science and Technology, 91* (1993), 1-3, pp. 95-117
[5] Tse, S. D., Anthenien, R. A., Miyasaka, K., Fernandez-Pello, A. C., An Application of Ultrasonic Tomographic Imaging to Study Smoldering Combustion, *Combustion and Flame, 116* (1999), 1-2, pp. 120-135
[6] Dosanjh, S. S., Pagni, P. J., Fernandez-Pello, A. C., Forced Co-Current Smoldering Combustion, *Combustion and Flame, 68* (1987), 2, pp. 131-142
[7] Buckmaster, J., Lozinski, D,. An Elementary Discussion of Forward Smoldering, *Combustion and Flame, 104* (1996), 3, pp. 300-310
[8] Leach, S. V., Rein, G., Ellzey, J. L., Ezekoye, O. A., A Numerical Study of Reverse Smoldering Combustion, *Combustion Science and Technology, 130* (1997), 1, pp. 247-267
[9] Ghabi, C., Benticha, H., Sassi, M., Numerical Study of Olive Waste Combustion in a Fixed Bed, *Physical and Chemical News, 19* (2004), pp. 53-59
[10] Ghabi, C., Rein, G., Benticha, H., Sassi, M., Bidimensionnal Numerical Model for Polyurethane Smoldering in a Fixed Bed, *Proceedings,* 4th International Conference on Computational Heat and Mass Transfer, Paris-Cachan, 2005, pp. 578-584
[11] Ghabi, C., Benticha, H., Sassi, M., Computational Modeling and Simulation of Forward-Smoldering of Porous Media in a Fixed Bed, *Progress in Computational Fluid Dynamics, 7* (2006), 5, pp. 283-293
[12] Bar Ilan, A., Rein, G., Fernandez-Pello, A. C., Torero, J. L., Urban, D. L., Forced Forward Smoldering Experiments in Microgravity, *Experimental Thermal and Fluid Science, 28* (2004), 7, pp. 743-751
[13] Di Blasi, C., Analysis of Convection and Secondary Reaction Effects within Porous Solid Fuels Undergoing Pyrolysis, *Combustion Science and Technology, 90* (1993), 5, pp. 315-321
[14] Di Blasi, C., Modeling and Simulation of Combustion Processes of Charring and Non-Charring Solid Fuels, *Progress in Energy and Combustion Science, 19* (1993), 1, pp. 71-104
[15] Kashiwagi, T., Nambu, H., Global Kinetic Constants for Thermal Oxidative Degradation of a Cellulosic Paper, *Combustion and Flame, 88* (1992), 3-4, pp. 345-368
[16] Shafizadeh, F. F., Bradbury, A. G. W., Thermal Degradation of Cellulose in Air and Nitrogen at Low Temperature, *Journal of Applied Polymer Science, 23* (1979), 11, pp. 1431-1442
[17] Chao, C. Y. H., Wang, J. H., Transition from Smoldering to Flaming Combustion of Horizontally Oriented Flexible Polyurethane Foam with Natural Convection, *Combustion and Flame, 135* (2001), 4, pp. 2252-2264
[18] Wang, J. H., Chao, C. Y. H., Kong, W., Experimental Study and Asymptotic Analysis of Horizontally Forced Smoldering Combustion, *Combustion and Flame, 135* (2003), 4, pp. 405-419
[19] Bilbao, R., Mastral, J. F., Aldea, M. E., Ceamanos, J., Betrán, M., Lana, J. A., Experimental and Theoretical Study of the Ignition and Smoldering of Wood Including Convective Effects, *Combustion and Flame, 126* (2001), 1-2, pp. 1363-1372
[20] Shult, D. A., Matkowsky, B. J., Fernandez-Pello, A. C., Forced Forward Smolder Combustion, *Combustion and Flame, 104* (1996), 1-2, pp. 1-26
[21] Leach, S. V., Rein, G., Ellzey, J. L., Ezekoye, O. A., Kinetic and Fuel Property Effect on Forward Smoldering, *Combustion and Flame, 120* (2000), 3, pp. 346-358
[22] Ergun, S., Fluid Flow through Packed Columns, *Chemical Engineering Progress, 48* (1952), 1, pp. 89-94
[23] Wakao, N., Kaguei, S., Heat and Mass Transfer in Packed Beds, Gordon Breach Science Publishers, New York, USA, 1982

[24] Incroprera, F. P., DeWitt, D. P., Fundamentals of Heat and Mass Transfer, *Proceedings*, 3rd ed., John Wiley & Sons, New York, USA, 1990
[25] Fatehi, M., Kaviany, M., Role of Gas-Phase Reaction and Gas-Solid Thermal Nonequilibrium in Reverse Combustion, *International Journal of Heat and Mass Transfer, 40* (1997), 11, pp. 2607-2620
[26] Patankar, S. V., Numerical Heat Transfer and Fluid Flow, Hemisphere Publishing Corporation, Washington D. C., USA, 1980
[27] Markovic, A., An Investigation of Sparse Matrix Solvers with Applications to Models of Transport in Porous Media, Ph. D. thesis, Queensland University of Technology, Brisbane, Australia, 1995
[28] Hanneke, M. R., Ellzey, J. L., Modeling of Filtration Combustion in a Packed Bed, *Combustion and Flame, 117* (1999), 4, pp. 832-840
[29] Siek, B. S. J., A Modern Framework for Portable High Performance Numerical Linear Algebra, Ph. D. thesis, University of Notre Dame, Notre Dame, Ind., USA, 1999
[30] Eisenstat, S. C., Gursky, M. C., Schultz, M. H., Sherman, A. H., The Yale Sparse Matrix Package the Symmetric Codes, *International Journal for Numerical Methods in Engineering, 18* (1982), 8, pp. 1145-1151

Authors' addresses:

C. Ghabi, H. Benticha,
Laboratoire d'Etudes des Systemes Thermiques et Energétiques,
Ecole Nationale d'Ingénieurs de Monastir
5000 Tunisie

M. Sassi
The Petroleum Institute
P. O. Box 2533, Abu Dhabi, UAE

Corresponding author C. Ghabi
E-mail: ghabichekib@yahoo.fr

Paper submitted: July 22, 2006
Paper revised: April 12, 2007
Paper accepted: October 30, 2007